Valley-mixing effects in short-period superlattices

Yan-Ten Lu and L. J. Sham
Department of Physics (B-019), University of California, San Diego, La Jolla, California 92093
(Received 13 February 1989; revised manuscript received 12 May 1989)

The subband structure of $(GaAs)_N/(AlAs)_M$ along the growth direction [001] through the center of the Brillouin zone and through the zone-boundary point at (100) is calculated using a second-neighbor tight-binding method using the parameters fitted to the conduction valleys of the bulk materials. The parentage of the states in the bulk Γ and X valleys is traced. A striking general feature of the valley mixing depending sensitively on N and M is explained in terms of the symmetry of the superlattice. This result forms a basis for exploring the lack of perfection of the interface.

I. INTRODUCTION

A GaAs/AlAs superlattice growth along the [001] axis with each period composed of N layers of GaAs and M layers of AlAs is considered a short-period superlattice if N and M are small, say less than 10. The conduction subbands are mainly determined by the confinement effect of a series of square wells simulating the difference in conduction-band edges of the two compounds. In addition, the short-period superlattice introduces a mixing of different conduction valleys, an effect which cannot be described by the simple Kronig-Penney model. This effect has been studied experimentally[1–15] and the superlattice band structure has been much studied theoretically.[16–35] The status to date is reviewed by Wilson.[36] What interests us here is the role of the interface in the valley mixing. In $GaAs/Al_xGa_{1-x}As$ superlattices and quantum wells in general, because the interfaces simply serve as potential barriers for the conduction electrons, not much information about the interface can be gleaned from a study of the conduction electrons. The phenomenon of valley mixing across the interface provides a means of investigating the interface effect on the conduction electrons beyond the effective-mass approximation. A simple model is constructed to connect the interface with the valley mixing. It demonstrates the potential for untangling experimental measurements of the valley mixing to yield information on the electron behavior across an interface.

Figure 1 shows the band-edge alignment along the growth axis (the z axis) of the superlattice. The valence-subband holes tend to be confined in the GaAs layers. The bulk Γ conduction-band edge is lower in the GaAs layers than in AlAs and, thus, tends to confine the conduction electrons to GaAs layers. The nesting of the Γ band gap of GaAs entirely within the AlAs gap makes the superlattice so-called "type I." On the contrary, the X conduction valleys of AlAs lie lower than those in GaAs, provided the valence-band offset is greater than 0.2 eV. The X conduction-subband electron tends to be confined in AlAs layers. If the energy of the X subband falls below the energy of the Γ subband, the staggered alignment of the X conduction-band edge and the Γ valence-band edge yields the "type-II" superlattice. If the GaAs layers are sufficiently thick, the Γ conduction subband lies below the X subband and the superlattice has a direct band gap. The transition from type I to type II has been studied by varying the relative layer thickness,[1,3,4,6,7,10–13] by applying electric field along the growth axis,[5,8,9] and by hydrostatic pressure[2] for uniaxial stress.[14,15] In the type-II case the lowest-energy optical transition becomes "indirect" in one of two senses: either the k vector in the superlattice Brillouin zone is changed, or the valence electron mainly in GaAs layers is excited to be mainly in the AlAs regions conserving the wave vector. The latter is also called "pseudodirect."[5] Such a transition is distinguished by the characteristics of lower optical efficiency, slower photoluminescence decay rate,[3] distinctive dependence on the longitudinal electric field,[5,8] different temperature dependence of energy gaps from that of the bulk GaAs gap,[1] and the g value from the optically detected magnetic resonance.[11]

Because of the anisotropy of the effective-mass tensor of AlAs at point X ($m_l=1.1$, $m_t=0.2$), the confined en-

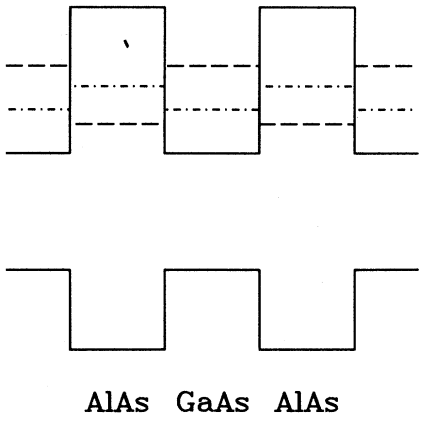

FIG. 1. Band-edge alignment of a GaAs/AlAs superlattice. The vertice energy axis is not to scale. Solid line denotes the Γ band edges, the dashed line the X band edges, and the dotted-dashed line the L band edges.

ergy level of X_z with the larger effective mass along the z axis is lower than that of X_x or X_y, with the smaller effective mass along the z axis. The alternating layers change the lattice symmetry in the z direction. The Bravais lattice of an N/M superlattice depends on the total number of layers in a period, $N+M$. If it is even, the lattice is primitive tetragonal; if it is odd, the lattice is body-centered tetragonal. The corresponding Brillouin zones are shown in Figs. 2(b) and 2(c). Different parts of the three-dimensional fcc Brillouin zone are folded into a superlattice Brillouin zone as shown in Fig. 2. There are two consequences: (1) The Γ electron wave function mixes with the X_z wave function, enhancing the "indirect" or "pseudodirect" transition from the valence subband to X_z, which is, strictly speaking, a direct transition in the superlattice. (2) In the case where both N and M (the numbers of layers of GaAs and AlAs in a period) are even, the degeneracy between X_x and X_y states is lifted because of the valley mixing.

Some experiments[3,12] suggest that, in the type-II regime, the lowest luminescence transition is from an $X_{x,y}$ level based on the argument that the X_z level, mixing with Γ, cannot have the observed decaying time behavior of the photoluminescence peak. This implies that the X_x and X_y mixing is strong enough to compensate for the energy difference with the X_z level due to the anisotropic effective mass. On the other hand, the electric field experiment[8] shows the X_z to be lower than the $X_{x,y}$ levels and obtains the mixing strength of the order of 1 meV between Γ and X_z. There is a similar controversy in theoretical papers.[27,29] We wish to add our own results on this point.

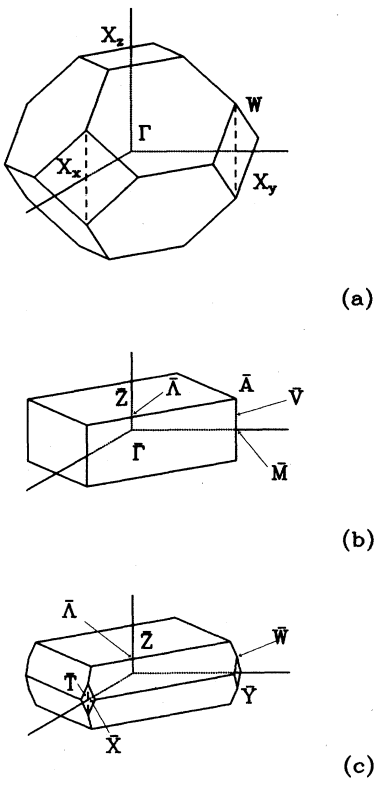

FIG. 2. (a) Brillouin zone of the bulk fcc structure. (b) Brillouin zone of a $(GaAs)_N/(AlAs)_M$ superlattice with even $N+M$. (c) Brillouin zone of the superlattice when $N+M$ is odd.

Computations of the subbands in the short-period superlattices have used the tight-binding method,[13,16,26–28] the Wannier function,[21,29] the pseudopotential method,[17,19,25,35] and the first-principles self-consistent local-density approximation (LDA).[22,30–34] The first-principles calculations using the LDA are unable to get the band gaps in the bulk correctly[37] without adjustments.[22,23] They are more suited to study problems involving the total energy such as the superlattice stability[30–32] than for the conduction subbands. Earlier calculations[16] starting with an empirical fit to the bulk bands took the valence-band offset to be 15% of the band-gap difference, and, thus, yielded no type-II alignment with the conduction X valley and no valley-mixing effects. Two recent papers specifically addressed the valley-mixing problem. Ihm[27] worked out a type-I and type-II phase diagram using a nearest-neighbor tight-binding model and found the $X_{x,y}$ level to be lower than the X_z level. This ordering of the X level is not valid since the complete neglect of the next-nearest-neighbor interaction in his tight-binding model gives an infinite transverse effective mass, m_t, in the X valley of the bulk bands, with the consequence that the $X_{x,y}$ levels always stay at the bottom of the bulk X valley, lower than the X_z level. Ting and Chang[29] used one-band Wannier functions, and found the Γ-X_z mixing and the X_z level to be lower than $X_{x,y}$. A disadvantage of the Wannier functions is the nonlocal nature (spanning 20 neighbors in their case). Thus, too many overlap Hamiltonian parameters are affected by the interfaces, and there is no physical basis for their adoption of the mean of the bulk parameters from the two compounds. Such a wide interface region greatly reduce the effective widths of the well and barrier regions. This feature makes the Wannier function an inappropriate method for studying the short-period superlattices. For example, the transition from type-I to type-II behavior was found by Ting and Chang to occur at 80 Å GaAs thickness, as compared with the expected[11] value of 35 Å. The one-band Wannier function is centered on a unit cell, in contrast to the tight-binding wave functions centered on atomic sites. This difference apparently leads to conclusions different from ours on the dependence on N and M of the symmetry of the states at the points of the superlattice Brillouin zone of high symmetry.

In this paper we present yet another theoretical study of the subbands of the short-period superlattice, to address specifically the issue of the Γ-X_z and X_x-X_y, valley mixings. The subband dispersion along the growth axis through X_x and the attendant symmetry analysis appear to have been done for the first time. The symmetry properties of the superlattice are investigated for arbitrary N and M. The different Bravais lattices described above for even and odd $N+M$ and, hence, the different Brillouin

zones (Fig. 2) lead to distinct band dispersions along the projection of a bulk X point, $\overline{A}-\overline{M}$ and $\overline{X}-\overline{Y}$ in Fig. 2. For even $N+M$, the $\overline{M}$ points along the x and y axes, being separated by a reciprocal-lattice vector, are equivalent points. For odd $N+M$, the $\overline{X}$ and $\overline{W}$ points whose difference is not a reciprocal-lattice vector are distinct points of the first Brillouin zone.

We adopt the tight-binding method including only second-nearest-neighbor interactions as the simplest and yet effective model to study the valley-mixing effects. We prefer this parametrization method to the first-principles self-consistent calculation because the fitting scheme is capable of reproducing more accurately the bulk conduction valleys at Γ and X including effective masses, which we believe are important indicators for the accuracy of the subbands and because its simplicity enables us to study more broadly the dependence on N and M. The disadvantage of the tight-binding parametrization method is the lack of knowledge of the parameters across the interface. We minimize this defect by keeping the range of next-nearest neighbors and by using as few cross-interface parameters as possible. We also study the dependence of the subbands on such parameters.

The resultant subbands along the growth axis through Γ and X_x show distinctive variations with the layer thickness N and M, which can be understood by a combination of symmetry analysis and consideration of the envelope functions. The sensitivity of the symmetry properties to the imperfections of the interfaces may in the future lead to information on the interface by comparing experiments with our calculated subbands.

Section II contains the symmetry properties of the superlattices. In Sec. III the tight-binding fit of the sp^3 model to the bulk band structures and the method of treating the tight-binding parameters across the interface are described. Section IV presents the mixing of the subbands originating from the Γ conduction-band valley of GaAs and the subbands originating from the X_z conduction-band valley of AlAs. Computed mixing strength is compared with experiment. Section V presents the mixing effects of the subbands from the AlAs X_x and X_y valleys. Section VI summarizes our results and discusses the perspective of our work on the ideal interface in the large context of real and imperfect interfaces.

II. SUPERLATTICE SYMMETRY

In this section we collect a number of important symmetry properties for an idealized superlattice with a period along the z axis of N layers of GaAs and M layers of AlAs, all atoms being on the sites of a zinc-blende lattice with lattice constant a. The coordinate axes are chosen as usual along the principal symmetry directions [100], etc.

Because of the inequivalence of the Ga and Al planes, of the point-group operations in T_d ($\bar{4}3m$), only those which do not change the z coordinates and those which involve reflections in some x-y planes or twofold rotations about the x or y axis survive as the point-group operations leaving the superlattice invariant, forming the D_{2d} ($\bar{4}2m$) point group.[38]

The Bravais lattice of the zinc blende is fcc. Viewed along the z axis, alternate planes of atoms of the same element do not lie on top of each other. The lattice vector covering one period of the superlattice points along the growth direction if $N+M$ is even and points along $(0,1,N+M)$ if $N+M$ is odd. Therefore, the Bravais lattices are different in the two cases. When $N+M$ is even, the Bravais lattice is simple tetragonal, with the basis vectors

$$(1,1,0)a/2,\quad (-1,1,0)a/2,\quad (0,0,1)(N+M)a/2\ , \tag{1}$$

where a is the bulk lattice constant. The space group, which is symmorphic, is[39] D_{2d}^5 ($P\bar{4}m2$). It is not[2,22] $D_{2d}^1(P\bar{4}2m)$ because the twofold axis in the x-y plane are [100] and [010], bisecting the basis vectors in the same plane, Eq. (1). When $N+M$ is odd, the Bravais lattice is body-centered tetragonal, with the basis vectors

$$(1,1,0)a/2,\quad (-1,1,0)a/2,\quad (0,1,N+M)a/2\ . \tag{2}$$

The space group, which is symmorphic, is D_{2d}^9 ($I\bar{4}m2$). The first Brillouin zone has a different shape from the simple tetragonal case. [See Figs. 2(b) and 2(c).]

We are interested in the subbands along $(0,0,fc^*)$ and $(a^*,0,fc^*)$, where

$$0\le f\le 1,\quad a^*=2\pi/a,\quad c^*=2\pi/a(N+M)\ . \tag{3}$$

Referring to Fig. 2, we put a bar over the symbol for a symmetry point in a superlattice Brillouin zone to distin-

TABLE I. Symmetry properties of superlattice $(GaAs)_N/(AlAs)_M$. $\mathcal{G}_0$ is the point group at vector $\mathbf{k}$.

$N+M$:	Even		Odd	
Bravais lattice:	simple tetragonal		body-centered tetragonal	
Space group:	D_{2d}^5 ($P\bar{4}m2$)		D_{2d}^9 ($I\bar{4}m2$)	
$\mathbf{k}(0\le q\le c^*)$	Notation	$\mathcal{G}_0$	Notation	$\mathcal{G}_0$
$(0,0,0)$	$\overline{\Gamma}$	D_{2d}	$\overline{\Gamma}$	D_{2d}
$(0,0,q)$	$\overline{\Lambda}$	C_{2v}	$\overline{\Lambda}$	C_{2v}
$(0,0,c^*)$	$\overline{Z}$	D_{2d}	$\overline{Z}$	D_{2d}
$(a^*,0,0)$	$\overline{M}$	D_{2d}	$\overline{X}$	D_2
$(a^*,0,q)$	$\overline{V}$	C_{2v}	$\overline{T}$	C_2
$(a^*,0,c^*/2)$	$\overline{V}$	C_{2v}	$\overline{W}$	S_4
$(a^*,0,c^*)$	$\overline{A}$	D_{2d}	$\overline{Y}$	D_2

TABLE II. The experimental band energies (O. Madelung, Ref. 43, and references therein) (in eV) and effective masses (in units of m_0) used to generate the tight-binding parameters of Table III.

Band edge	GaAs	AlAs	Mass	GaAs	AlAs
Γ_{15v}	0	−0.55	m_v	−0.51	−0.41
X_{5v}	−2.8	−2.9			
X_{3v}	−6.7	−6.15			
Γ_{1c}	1.52	2.58	m_c	0.067	0.15
X_{1c}	2.1	1.68	$m_{x\parallel}$	1.8	1.1
			$m_{x\perp}$	0.257	0.19

guish it from the three-dimensional case. The point groups associated with the various symmetry points for the superlattices are given in Table I. The two intervals of interest are related to the bulk conduction valleys at Γ and X_z and to be valleys at X_x and X_y, respectively. The consequences of the difference in symmetry along $(a^*,0,q)$ between the states labeled $\bar{X},\bar{T},\bar{W},\bar{Y}$ for odd $N+M$ and $\bar{M},\bar{V},\bar{A}$ for even $N+M$ in Table I will be shown in Sec. V.

The space-group operations can be divided into those not changing the z coordinate (denoted by E) and those changing z to $-z$ (denoted by J). An As plane between a Ga and an Al plane may be regarded as an interface plane between a GaAs region and an AlAs region. For an operation of J, the origin is at an atom equidistant from two nearest interface planes of As. For definiteness, the origin will be chosen to be the midpoint in an AlAs region. Thus, it is at an As atom if M is even and at an Al atom if M is odd. The representations in the bulk will always be referred to the origin at an As atom as is the convention. If we number the layers along the z axis (each layer consisting of an anion plane and a cation plane), an even-numbered layer and an odd-numbered layer are staggered relative to each other, whereas two layers, both even or odd numbered, lie directly on top of each other. When M is even, an operation of J brings an even- (odd-) numbered As plane to another even- (odd-) numbered As plane and an even-numbered cation (Al or Ga) plane to an odd-numbered cation plane of the same species. When M is odd, the roles of the cation and anion planes are reversed. Thus, when a point group contains elements of J, the symmetry properties of the states are different for even and odd M, in addition to the difference due to $N+M$ being even or odd. The effects of this difference will become apparent in Sec. V.

In a number of symmetry points, such as $\bar{\Gamma}$ and $\bar{A}$, we are interested in states with irreducible representations of unity under operations in E and ± 1 under J, which will be referred to as even- and odd-parity states, respectively.

III. TIGHT-BINDING MODEL FOR THE SUPERLATTICE

The sp^3 local orbitals[40] (S_i,Z_i,X_i,Y_i), with $i=a$ for the anion (As) and $i=c$ for the cation (Ga or Al), are used as the basis functions in the tight-binding model. In the traditional tight-binding method,[40–42] the energies at the high symmetry points in the Brillouin zone, e.g., Γ, X, and L, are used to fix the tight-binding parameters. However, this yields overly large band masses in the Γ and X valleys for the sp^3 model.[16] To produce the superlattice subbands in the energy range near the Γ and X conduction-band edges and the Γ valence-band edge, the tight-binding parameters must be accurate enough to reproduce these bulk band edges and the associated effective masses. The higher or lower bulk bands are not important. Therefore, instead of fitting to a number of valence and conduction bands, we concentrate on the highest valence band and lowest conduction band. We fit the conduction energy minima at points Γ and X and the highest valence-band edge and their associated masses for both bulk GaAs and AlAs.[43] We neglect the spin-orbit coupling and fit only the heavy-hole band edge and effective mass. We also neglect the "camel-back" feature at X since the height of the "camel back"[44] is at least 1 order of magnitude less than the zero-point energy in the X quantum well. The term values of AlAs are uniformly shifted down 0.55 eV to yield the valence-band offset at 34% of the direct-band-gap difference between AlAs and GaAs, in accordance with the photoluminescence data.[3,45]

The experimental values of the band edges and effective masses used are listed in Table II and the resultant bulk tight-binding parameters for the Hamiltonian are listed in Table III. In the Slater-Koster notation, the subscripts 0 and 1 refer to the anion (As) and the cation (Ga or Al) respectively. In order to minimize the number of overlap parameters between Ga and Al across an interface, we

TABLE III. Tight-binding parameters (in eV) in Slater-Koster (J. C. Slater and G. Koster, Ref. 40) notation.

SK notation	GaAs	AlAs
$E_{ss}(000)_0$	7.0012	6.7878
$E_{xx}(000)_0$	−0.6498	−0.0908
$E_{ss}(000)_1$	7.2004	5.5530
$E_{xx}(000)_1$	5.7192	5.4933
$E_{ss}(\frac{1}{2}\frac{1}{2}\frac{1}{2})$	0.6084	0.4657
$E_{sx}(\frac{1}{2}\frac{1}{2}\frac{1}{2})_{01}$	−0.6375	−0.4981
$E_{sx}(\frac{1}{2}\frac{1}{2}\frac{1}{2})_{10}$	1.8169	1.8926
$E_{xx}(\frac{1}{2}\frac{1}{2}\frac{1}{2})$	−0.5586	−0.5401
$E_{xy}(\frac{1}{2}\frac{1}{2}\frac{1}{2})$	−1.2224	−1.4245
$E_{ss}(110)_0$	−0.3699	−0.2534
$E_{sx}(110)_0$	−0.5760	−0.8941
$E_{xx}(110)_0$	0.2813	0.1453
$E_{xx}(011)_1$	−0.6500	−0.7912

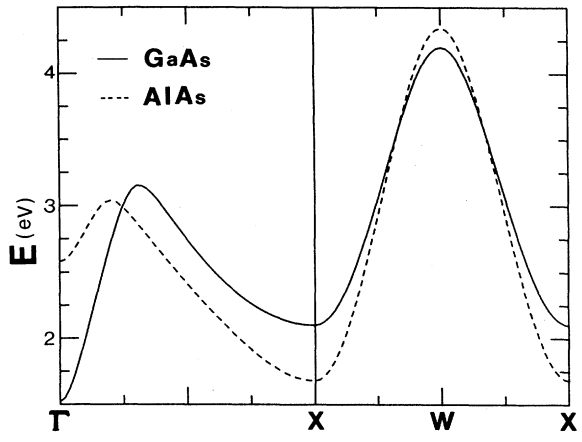

FIG. 3. Band structures for the bulk compounds along (001) and (10k).

keep only one second-neighbor interaction between cations that is indispensible in the bulk in yielding the correct dispersion in the transverse direction of the X valley. The bulk conduction bands along $(0,0,K_z)$ and along $(a^*,0,K_z)$ calculated from these parameters are plotted in Fig. 3 for both GaAs and AlAs. This figure clearly illustrates the conduction-band–edge alignment at Γ and X. The resultant bands yield the lowest Γ_{15} conduction-band energies for GaAs and AlAs in good agreement with experiment, but the X_3 energy is too high for GaAs and for AlAs by 7 and 5 eV, respectively. The errors in X_3 do not affect the superlattice subbands in the energy range between the two conduction-band edges, which are of Δ_1 character.

A superlattice electron state with wave vector (K_x,K_y,K_z) and energy E is a linear combination of all the bulk states with the same K_x, K_y, and energy E, but different z components of the wave vector, denoted K_z. Here, we are particularly interested in the dispersion along $(0,0,q_z)$ and $(a^*,0,q_z)$, chosen to demonstrate the effect of Γ-X_z mixing and of X_x-X_y mixing, respectively. (See Fig. 2.)

A superlattice electron wave function at each pair of cation (Ga or Al) and anion (As) planes is expressed in terms of the basis set of the eight Bloch waves of sp^3 orbitals in the same plane with wave vector (K_x,K_y). In the second-neighbor interaction model the secular equation can be expressed in terms of coupling of one layer of a compound (two planes of atoms) to the two neighboring layers by means of two 8×8 transfer matrices.[46,47] The transfer matrices in the interior region of a compound are the same as the bulk ones. The transfer matrices across an interface are different from the bulk matrices of either host (see below). For thick layers it is computationally more efficient to express the superlattice wave function in the interior of a layer in terms of the Bloch waves (both propagating and evanescent) of the bulk, connected to the wave function in the next layer by the transfer matrices at the interface, thus leading to a secular matrix for the coefficients of the bulk Bloch waves.

Along the symmetry direction $(0,0,q)$, the 8×8 transfer matrix can be reduced to one 4×4 matrix and two 2×2 matrices. The wave functions of the lowest set of conduction subbands are expressible in terms of the basis set of S_a,Z_a,S_c,Z_c, with symmetry $\bar{\Lambda}_1$ (corresponding to the Δ_1 in three dimensions), and those of the highest set of valence subbands are linear combinations of the degenerate set of $X_a\pm Y_a$ and $X_c\pm Y_c$, with symmetry $\bar{\Lambda}_4$ and $\bar{\Lambda}_3$ (corresponding to Δ_4 and Δ_3). Along $(a^*,0,q)$, where there is a mixture of the states in the X_x,X_y valleys, the basis set for the wave function can also be reduced to S_a,Z_a,X_c,Y_c (which are compatible with X_1).

Within this model, with a limited number of second-neighbor parameters, as listed in Table III, further simplifications can be made for numerical work: (1) two of the coefficients of the four local orbitals can be expressed in terms of the other two and, thus, the transfer matrices are reduced to 2×2; (2) the bulk dispersion relations can be expressed as quadratic forms of $\cos(ka)$ or $\cosh(ka)$ with the coefficients as functions of energy. The bulk eigenequations can be solved analytically for a given energy, thereby greatly increasing the computational speed and accuracy.

Across an ideal GaAs/AlAs interface, planes of atoms are arranged in the order

$$\text{As Ga} \cdots \text{As Ga } \underline{\text{As}} \text{ Al} \cdots \text{As Al}\ .$$

The As plane (underlined) between the Ga plane and Al plane is the interface. The tight-binding parameters in our model affected by the interface are two on-site arsenic energies, $E_{ss}(000)_0$ and $E_{xx}(000)_0$ and two in-plane second-neighbor interactions $E_{ss}(110)_0$ and $E_{xx}(110)_0$ [needed along $(0,0,q)$], and a cross-interface interaction between Ga and Al, $E_{xx}(011)_1$ [needed in addition to the first four parameters along $(a^*,0,q)$]. All other parameters are given by the bulk values. We choose the mean values between the GaAs and AlAs bulk values for the five parameters affected by the interface. We have also studied the subband energies as functions of these interface parameters varied between the bulk values. The subband energies are not sensitive to these parameters, except for N or M less than 3.

We are interested in the X subbands between the bottom of the AlAs X valley and the bottom of the GaAs X valley, i.e., between 1.68 and 2.1 eV, and in the corresponding Γ-X mixing. In the following two sections we present the calculated superlattice electron energies in this range. The energies are computed either by directly solving the $4(N+M)\times4(N+M)$ matrices for superlattices with small N and M (≤5), or by looking for zeros in the secular equations of the expansion coefficients of the bulk Bloch waves for superlattices of larger periods. The overlapping regime where both methods pertain serves as a check for our numerical work.

Because the tight-binding parameters are generated from the bulk bands near the band gap, our s-orbital energies are closer to the s^*-term values[42] than the s orbitals in the sp^3s^* model. The conduction Γ valley has a stronger anionic S_a component than the sp^3s^* model.

Consequently, our estimate of the Γ-X mixing is stronger than the conventional tight-binding model. Furthermore, the lack of self-consistency of the interface parameters means that the results presented in the following sections for the very-short-period superlattices may be unreliable. Our calculation is probably valid for N/M greater than 3, based on the comparison of the calculated energy gap of $(GaAs)_N/(AlAs)_N$ superlattices with experiment.

IV. Γ-X VALLEY MIXING

Figure 3 helps one visualize a superlattice state with wave vector $(0,0,q_z)$ as a linear combination of bulk states at the same energy in the following way. For the energy below the bottom of AlAs X valley, 1.68 eV, the superlattice wave function consists of propagating and evanescent waves in the GaAs layers and only evanescent waves in the AlAs layers. In the energy range 1.68–2.1 eV, the eigenfunction consists of Bloch waves from both the GaAs Γ valley and the AlAs X_z valley, and also evanescent waves from the AlAs Γ valley and the GaAs X_z valley. The mixing allows the optical transition between states that, in the effective-mass approximation, would be termed the GaAs Γ valence subband and the AlAs X conduction subband. In this section we present the calculated results of states with zero in-plane wave-vector components within this energy range in the superlattice $(GaAs)_N/(AlAs)_M$, referred in the figure as the N/M superlattice.

In Fig. 4 we plot the conduction-subband energies at $\bar{\Gamma}$ as functions of N for the $(GaAs)_N/(AlAs)_N$ superlattice. By comparing with the effective-mass results using the square wells as shown in Fig. 1, and by examining the wave functions that are dominant in the GaAs or AlAs region, we identify the levels as from the Γ or X_z valley, denoted $n\Gamma$ and nX with $n=0,1,2\ldots$. Note that, because the Γ-valley effective mass is small, the Γ levels are more widely spaced and increase in energy more rapidly as N decreases than the X levels. The parity is defined at the end of Sec. II. The even- (odd-) parity states have an irreducible representation $\bar{\Gamma}_1$ ($\bar{\Gamma}_3$), following the number system of Koster.[38] The coefficients of the S orbitals have the same parity as the state, and those of the Z orbitals have the opposite parity. Each Γ level retains the same parity as N varies, but the parity of each X level alternates for successive N's. The lowest level, $0X$, has the same parity as the integer N. The parity behavior may be understood with the help of the effective-mass approximation, in which an eigenfunction is the product of the bulk wave function at a band edge and the envelope function. The parity of the superlattice state is the product of the parity of the bulk band-edge state and the parity of the envelope function. The bulk Γ state has a zero wave vector along the z axis and, therefore, constant coefficients for the basis set of orbitals (S_a,Z_a,S_c,Z_c) over the GaAs region of a supercell. The superlattice Γ level, thus, has the same parity as the envelope wave function. On the other hand, the bulk X state with wave vector $(0,0,a^*)$ has zero coefficients for (Z_a,S_c) and alternating ±1 as coefficients of (S_a,Z_c) in the AlAs region. In the AlAs region with M layers, the ratio of the coefficients of S_a on the two interface As planes is $(-1)^M$. Thus, for the even-parity envelope functions of the $(2n)X$ levels, the parity of the state is the same as that of M and, for odd-parity envelope functions of the $(2n+1)X$ levels, the parity of the state is opposite that of M. Thus, the parity behavior of the X levels shown in Fig. 4 is explained.

At $N=16$, the crossing of the 1Γ level and the $4X$ level results in a degeneracy because the different in parity forbids any mixture. The lowest-level anticrossing occurs at $N=12$ (34 Å), which agrees with the expected GaAs thickness of the type-II–to–type-I superlattice transition.[11]

The M dependence of the parity of the X levels is in agreement with the occurrence of the Γ-X splitting in Ref. 2, but it appears to contradict the results of Ting and Chang.[29] The difference is not just semantic since the anticrossing with the Γ levels depends on the parity. The conflict may have originated from the difference in the choice of the center of the z to $-z$ inversion operation (one of the J's in Sec. II). In the atomic-orbital representation, the As plane between the Ga plane and the Al plane naturally becomes the interface boundary and the center of inversion is at an atomic plane midway between two As interface planes. In the Wannier approach of Ref. 29, the center appears to be at the midpoint between cation and anion. If distinction between the cation and anion sites is not made in the Wannier orbital, then the parity result is incorrect. The reversal of parity relative to M would also occur if X_1 is defined relative to the cation at the original instead of the conventional anion.

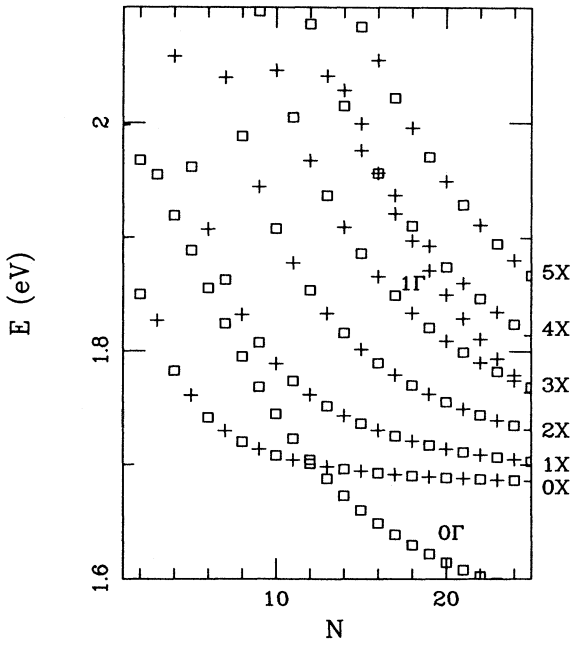

FIG. 4. Energy levels at $\bar{\Gamma}$ as functions of N for the $(GaAs)_N/(AlAs)_N$ superlattices. Labels $n\Gamma$ and nX denote the number of a level and its origin in bulk conduction valley. An open square denotes even parity and a cross odd parity.

Our calculated band gap of the $(GaAs)_N/(AlAs)_N$ superlattice as a function of N, shown as curves joining the discrete points at integer values of N in Fig. 5, is compared with experiments. The solid curve is from the lowest conduction Γ level to the highest valence subband and the dashed curve is from the lowest conduction X level. Correction of the experimental gap by the excitation binding energy has not been made since it is negligible compared with the spread of experimental data from different groups. Theory shows that the lowest transition is the direct Γ-to-Γ one for N greater than 12 and is the "pseudodirect" one from Γ to X for N less than 12. This is in very good agreement with experiment. The actual band values are in fair agreement with experiment, except for $N<3$. We do not believe that our bulk-fit tight-binding parameters can represent GaAs or AlAs regions only one or two layers thick.

We also compare the calculated transition energies with experimental data for two different series of $(GaAs)_N/(AlAs)_M$ superlattices, with $N=8$ as functions of M and with $M=5$ as functions of N (Fig. 6). There is again good agreement, especially in the direct-to-pseudodirect transition at $(GaAs)_8/(AlAs)_5$.

The scatter of experimental data is much larger than the difference between the results of our tight-binding calculation and of the Kronig-Penney model for separate square wells of the Γ and X valleys. In Fig. 7 we compare the tight-binding energies at $\bar{\Gamma}$ with the Kronig-Penney model for the series of $(GaAs)_N/(AlAs)_M$ with $M=7$ as functions of N. The Γ levels from the latter are given by the dashed curves. The results from the Kronig-Penney model for the flat X levels are not shown since they are almost indistinguishable from the tight-binding results. The Kronig-Penney model cannot, of course, reproduce the Γ-X mixing. The parity dependence of the X levels on M described above is again confirmed. There is degeneracy when two levels of different parity cross and there is a gap if the levels have the same parity. When M is increased from 7 to 8, the nX levels change their parities.

We have also computed the energies at $\bar{Z}(00c^*)$ as functions of N for the $M=7$ superlattices. For a state at $\bar{\Gamma}$, the wave function is the same on the two As interface planes which form the supercell boundaries and changes sign or not at the As interface plane in between, depending on whether the parity of the state is odd or even. The wave function has the same parity in the GaAs and AlAs regions, which is then unambiguously the parity of the state. Thus, the center of the inversion operations J could be chosen in either the GaAs or AlAs region. Such is not the case for the $\bar{Z}$ point. Because of the finite wave vector along z, the wave function changes sign from one boundary plane of the supercell to the other. If the wave function is even in the GaAs region, it has to be odd in the AlAs region and vice versa. The parity of the state must be defined with respect to a fixed center of inversion, which we have chosen to be the atomic plane in the middle of an AlAs region. The behavior of the wave

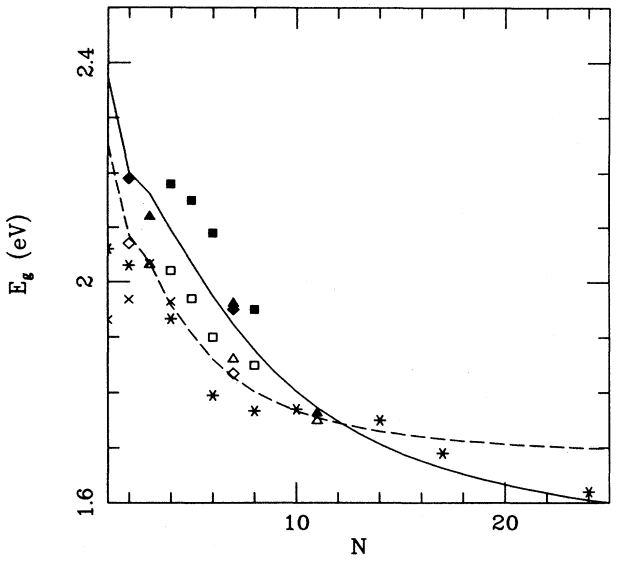

FIG. 5. Comparison of the calculated energy gaps of the $(GaAs)_N/(AlAs)_N$ superlattices (solid line for the direct Γ-to-Γ gap, dashed line for the pseudodirect Γ-to-X gap) with experiment: *, data from Ref. 1; ◇ and ×, Ref. 6; △, Ref. 3; □, Ref. 10.

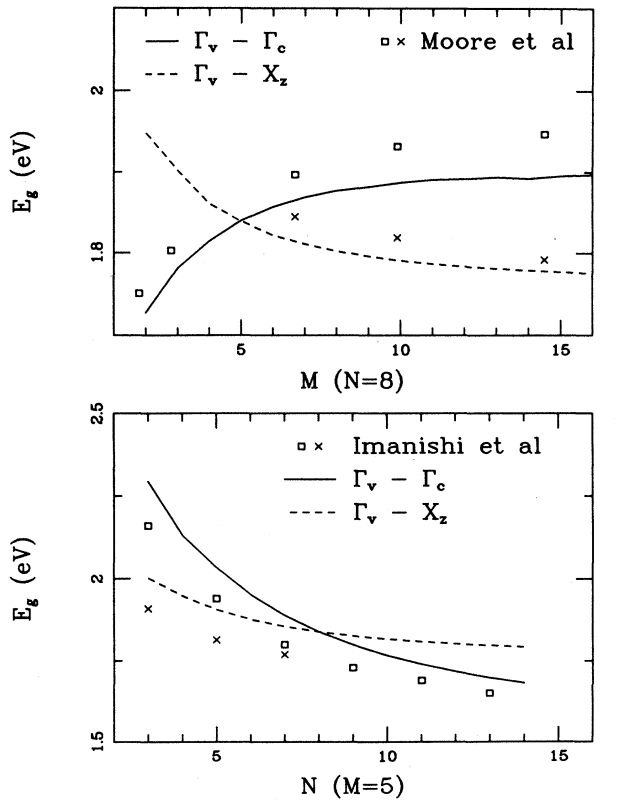

FIG. 6. Comparison of the calculated direct and pseudodirect energy gaps for the $(GaAs)_8/(AlAs)_M$ superlattices with the data of Ref. 10 and for the $(GaAs)_N/(AlAs)_5$ superlattices the data from Ref. 13.

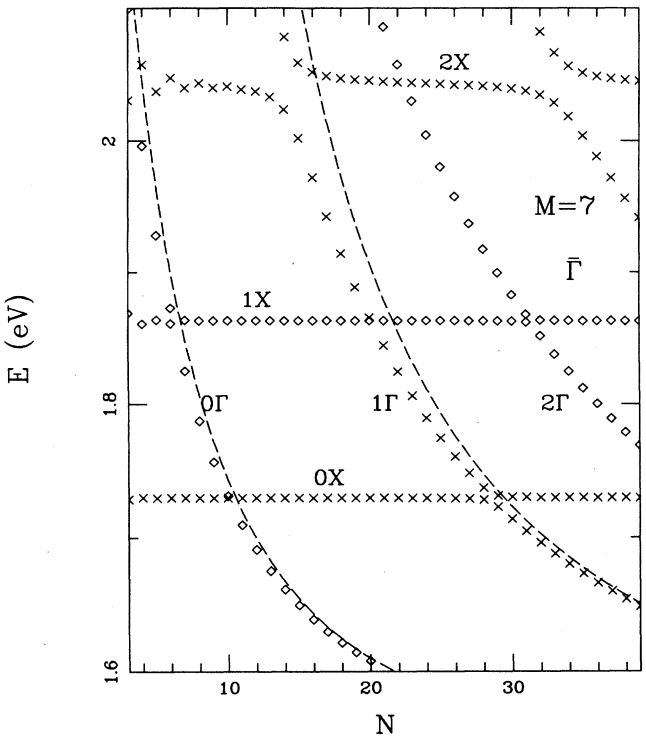

FIG. 7. Calculated energy levels for the $(GaAs)_N/(AlAs)_7$ superlattices at $\bar{\Gamma}$. ◇—even parity, ×—odd parity. The lowest two levels from the Kronig-Penney model for the Γ valley are shown (dashed lines) for comparison.

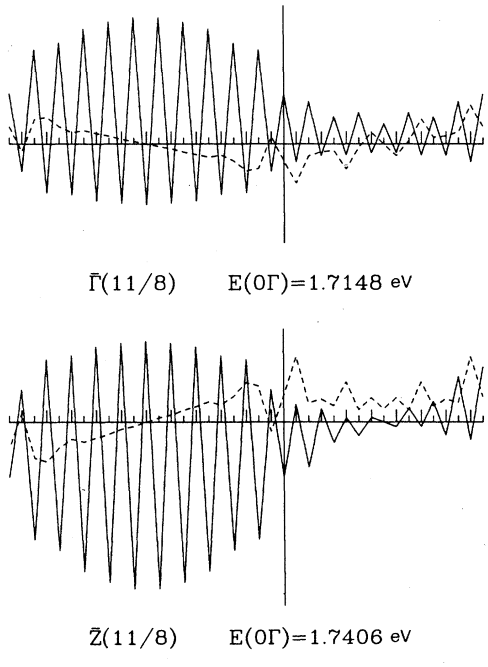

FIG. 8. Tight-binding coefficients of the orbitals, S_a, S_c (connected by the solid line) and of Z_a, Z_c (dashed line), for the wave functions of the level 0Γ at $\bar{\Gamma}$ and at $\bar{Z}$ in the $(GaAs)_{11}/(AlAs)_8$ superlattice. The anions locate at the short tic marks and cations at the long tic marks.

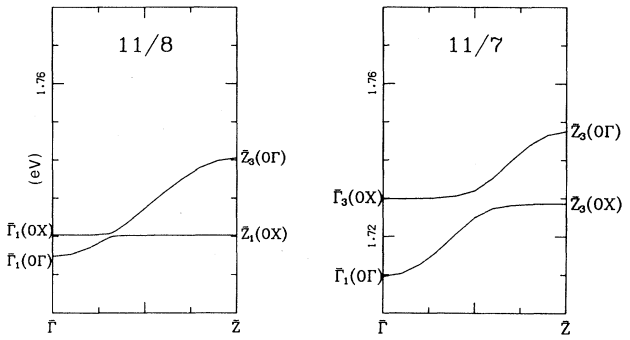

FIG. 9. Band structure along [001] for superlattices $(GaAs)_N/(AlAs)_M$ with $(N,M)=(11,8)$ and $(N,M)=(11,7)$.

functions of a Γ level at $\bar{\Gamma}$ and at $\bar{Z}$ for a $(GaAs)_{11}/(AlAs)_8$ superlattice, shown in Fig. 8, bears out the arguments above. Note that the parity of the dominant region does not change as q_z goes from 0 to c^*. This can be understood from the effective-mass approximation, where the envelope function determines the energy of the state.

The states have no well-defined parties when q_z is not equal to either 0 or c^*, and splitting always occurs whenever a Γ subband crosses an X subband. Figure 9 shows the subband structures along $\bar{\Gamma}$-$\bar{Z}$ for superlattices $(GaAs)_{11}/(AlAs)_8$ and $(GaAs)_{11}/(AlAs)_7$. While the X bands are flat, the Γ bands have bandwidths of tens of meV. The wave functions are strongly mixed near the anticrossings.

To compare the calculated magnitude of the Γ-X mixing with experiment, we note that Meynadier *et al.*[8] obtained a splitting of about 2.5 meV by applying an electric field to bring the X level into coincidence with the Γ level in a superlattice with a period of 35 Å GaAs and 80 Å AlAs, (approximately $N=12$, $M=28$). This is roughly equivalent to bringing the AlAs width to $M=12$, where the two levels would coincide. The calculated splitting for the $(GaAs)_N/(AlAs)_N$ superlattices near $N=12$ is about 1.7 meV. There is an order-of-magnitude agreement, which is quite good, considering the asymmetric potential well created by the electric field tends to push the Γ and X wave functions closer together.

V. VALLEY MIXING BETWEEN X_x AND X_y

The lowest conduction bands of bulk GaAs and AlAs along $a^*(1,0,f)$, where $0 \le f \le 1$, i.e., $X_x - W - X_y$, are plotted in Fig. 3. The end point $a^*(1,0,1)$ is connected to $a^*(0,1,0)$ by a fcc reciprocal-lattice vector, and is thus X_y. The superlattice potential mixes the two valleys. A superlattice wave function with wave vector $(a^*,0,q)$ in the energy range 1.68–2.1 eV is a linear combination of four propagating Bloch waves in the AlAs region and four evanescent waves in the GaAs region. The four propagating waves include a pair of waves moving in op-

posite directions from the X_x valleys and a pair from X_y.

The symmetry of the state with wave vector $(a^*,0,q)$, $0 \le q \le c^*$, depends on N and M, the number of GaAs and AlAs layers in a period.

Case I. N and M both even: If we adopt the numbering system of the irreducible representations[38] of the bulk Δ for the point group of $\bar{V}$, the state of $\bar{V}_1$ has the basis set

$$S_a(2l),\ Z_a(2l),\ X_c(2l)+Y_c(2l),\ X_c(2l+1)-Y_c(2l+1). \tag{4}$$

where the wave functions are sums of orbitals over the x-y planes with the in-plane wave vector $(a^*,0)$. The numbering of the atomic planes is explained in Sec. II. The state with symmetry $\bar{V}_2$ has the basis set

$$S_a(-2l+1),\ Z_a(-2l+1),\ X_c(-2l)-Y_c(-2l),\ X_c(-2l+1)+Y_c(-2l+1)\ . \tag{5}$$

Note the remarkable features of the s and z orbitals occurring only in alternate anion planes and of the $x \pm y$ orbitals rotating 90° from one cation plane to the next. The two states correspond, respectively, to the mixtures $X_x \pm X_y$. The superlattice potential provides the splitting, as shown in Fig. 10(a). At the end point $\bar{M}$, there is added inversion symmetry. The wave function of the lowest state is given in Fig. 11(a), illustrating the behavior of Eq. (4).

Case II. N and M both odd: The same two basis sets given by Eqs. (4) and (5) now have symmetry $\bar{V}_4$ and $\bar{V}_3$, respectively. The difference is due to the change of origin from As in case I to Al in the present case. Under an inversion J, these states transform into each other. Thus, these subbands are doubly degenerate. This is compatible with the double degeneracy at the end point of $\bar{M}_5$. This is borne out by the calculation for the $(GaAs)_7/(AlAs)_{11}$ superlattice shown in Fig. 10(b). The wave-function behavior is demonstrated in Fig. 11(b), a mirror image of this wave function giving another state with the same energy.

The change of the subbands from nondegenerate to doubly degenerate as N and M change from both even to both odd is illustrated in Fig. 12, where we plot the lowest four confined levels at $\bar{M}$ of the $(GaAs)_N/(AlAs)_N$ superlattice as functions of N. Again, this is reverse of the results of Ref. 29 and the explanation is the same as above. The energy of the lowest level is compared with the results of the Kronig-Penney model of the $X_{x,y}$ valleys with the same effective masses. The slightly higher energies from the tight-binding calculation are due to the averaging of the second-neighbor parameter between Ga and Al across the interface As plane, which reduces the width of the AlAs well. By contrast, the comparison between the tight-binding results and the Kronig-Penney model for the Γ and X_z levels is better because the

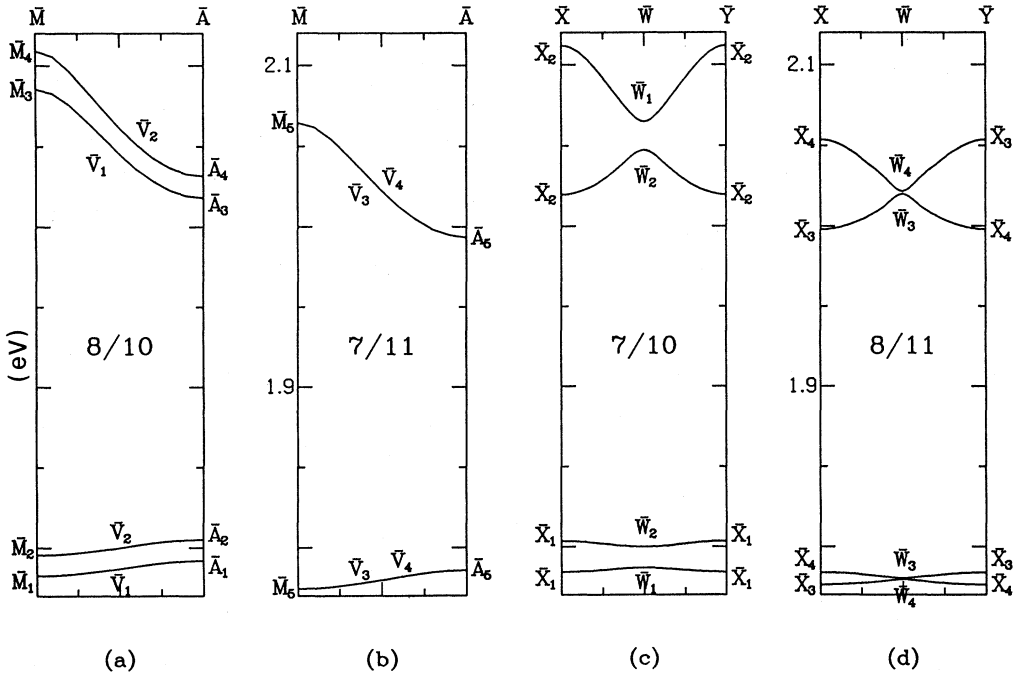

FIG. 10. Band structure along $(a^*,0,fc^*)$ for superlattices $(GaAs_N)/(AlAs)_M$ with (a) $(N,M)=(8,10)$, (b) $(N,M)=(7,11)$, (c) $(N,M)=(7,20)$, and (d) $(N,M)=(8,11)$.

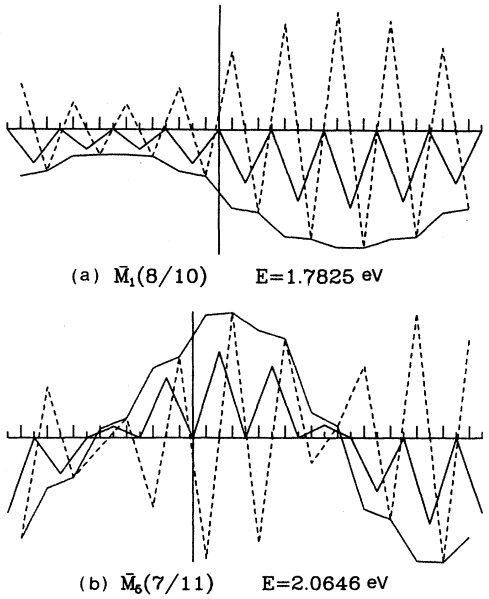

FIG. 11. (a) Tight-binding wave function for the state $\overline{M}_1$ in the $(GaAs)_8/(AlAs)_{11}$ superlattice. The s waves are linked by the solid line, p_x by the dotted line, and p_y by the dashed line. (b) The wave function of state $\overline{M}_5$ in $(GaAs)_7/(AlAs)_{11}$ superlattices.

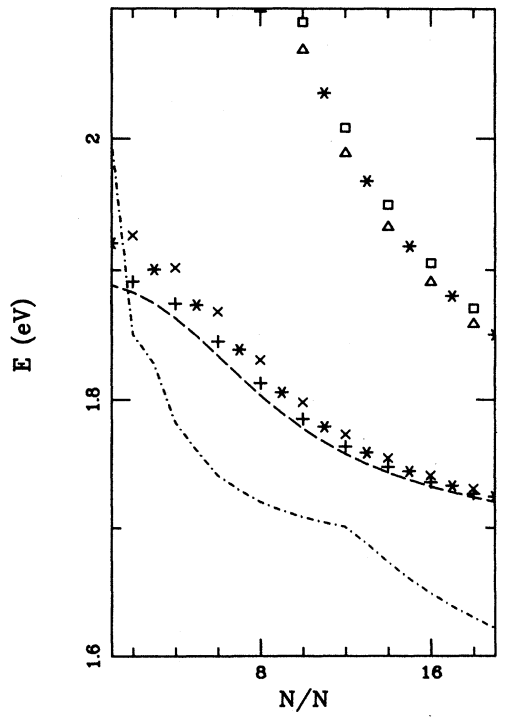

FIG. 12. Energies of the lowest four levels of the $(GaAs)_N/(AlAs)_M$ superlattices at $\overline{M}$ compared with the lowest level from the Kronig-Penney model of the X_x valley (dashed line) and with the lowest level at Γ from the tight-binding model (dotted-dashed line). +, state of symmetry $\overline{M}_1$; ×, $\overline{M}_2$; △, $\overline{M}_3$; □, $\overline{M}_4$; *, doubly degenerate states $\overline{M}_5$.

second-neighbor interactions occur entirely in the interface As plane for that symmetry direction (sec. IV). In Fig. 12 we also compare the $X_x \pm X_y$ energies with the lowest level of Γ-X_z from Fig. 4. The former energies are higher, except for $N=1$. This indicates the lowest type-II optical transition is from the X_z valley of AlAs to the GaAs valence subband for $N>1$.

Case III. N odd and M even: The general point $\overline{T}$ has only one nontrivial symmetry operation: the twofold rotation about the z axis. Compatible with the bulk X_1 is the even representation $\overline{T}_1$, with the basis set

$$S_a(l),\quad Z_a(l),\quad X_c(l),\quad Y_c(l)\ . \tag{6}$$

The end points are $\overline{X}$ and $\overline{Y}$, which have the same symmetry by the tetragonal rotation. Thus, the subbands are symmetrical about the midpoint $\overline{W}$. The bands may be thought of as ones arising from the X_x and X_y valleys crossing at $\overline{W}$, where the valley mixing splits the bands by degenerate perturbation theory. Actually, at the end points there is a certain amount of mixing, but not of equal strength. The subband structure is illustrated by the $(GaAs)_7/(AlAs)_{10}$ superlattice in Fig. 10(c).

Case IV. N even and M odd: The same basis set as Eq. (6) now has symmetry $\overline{T}_2$. The behavior is qualitatively similar to case III, except the splitting is smaller, as shown in Fig. 10(d). The states at $\overline{W}_4$ and $\overline{W}_3$ correspond to the bulk $X_x \pm iX_y$.

The marked difference as N or M changes is due to the change in symmetry. We have studied different series of $(GaAs)_N/(AlAs)_M$ superlattices by fixing N (M) and varying M (N). The variation of the band structures and of the symmetry properties of the wave function is in accordance with the analysis described above.

VI. SUMMARY AND DISCUSSION

We have used a tight-binding model with parameters obtained from the bulk bands to calculate the subband structures of $(GaAs)_N/(AlAs)_M$ superlattices along the growth direction through Γ and X_x for a variety of values of N and M. Tight-binding parameters across an interface are taken to be the average of the values from the two bulk regions. The important features of the bulk bands that have to be reproduced are the energies of the conduction valleys relative to the top of the valence band and the associated effective masses. The most striking common thread running through the results is the qualitative change as M or N varies by unity. All such changes can be understood by a symmetry-group analysis, together with consideration of the effective-mass envelope wave functions. The Bravais lattice changes from simple to body-centered tetragonal as $N+M$ changes from even to odd. The symmetry operations that change the sign of the z coordinates preserve the registry of the anion planes and shift the cation planes to their staggered counterparts when M is even and vice versa when M is odd. Thus, the symmetry properties of the states also change depending on whether M or N is even or odd.

Such sensitive dependence of the electronic properties

on N or M deduced by the theoretical analysis of the perfect superlattices forms a good basis for inferring the properties of the interface. For example, the Γ-X_z mixing in the vicinity of the level crossing is stronger for even M and weaker for odd M. This follows from the fact that the parity of the state at $\bar{\Gamma}$ from the X_z valley in the AlAs region correlates with M, while the parity of the lowest Γ level predominantly in the GaAs region is always even. Therefore, if the decay time of the pseudodirect transition is due to the valley mixing in a perfect superlattice, we expect that it will vary by about an order of magnitude as M goes from even to odd. Such strong dependence on M is removed if the transition is due to interface disorder scattering.[3,12]

The striking dependence of the subbands along $(a^*,0,fc^*)$ on N and M is typified in Fig. 10. Because such variations with N and M come from the symmetry dependence of the mixing of the X_x and X_y valleys in the perfect superlattices, imperfect interfaces may change such properties. Experimental observations of the mixing of these $X_{x,y}$ levels as N or M changes by unity will tell us a lot, then, about the interface. The next theoretical task is to examine the effects of models of imperfect interfaces[48] on the symmetry properties of such electronic states.

The agreement of the calculated energy gaps of the $(GaAs)_N/(AlAs)_N$ superlattices with experiment is quite good. The transition from type I to type II occurs at $N=12$, about where the effective-mass approximation predicts. The strength of the Γ-X mixing is of the same order as experiment. In the type-II region the X_z level lies below the $X_{x,y}$ levels, except when $N=1$.

The subband energies depend on the range of the effect of the interface on the electrons. The subbands along (001) in our model involve second-neighbor interactions only in the As interface plane and, thus, are effectively under the influence of an interface one atomic plane thick. The energies are in good agreement with the effective-mass approximation, except for the fine features of the valley mixing. Along the line $(1,0,f)$, the tight-binding parameters effectively involve the Ga and Al planes on either side of the As interface plane. The subband energies are raised relative to the effective-mass values. If more distant interaction parameters are affected by the interface, then the effective thickness of the interface increases and the subband energies increase also. Disorder in the interface could also increase the effective thickness of the interface in the same sense.

The simplicity of the tight-binding model has enabled us to explore the remarkable dependence of the valley mixing between Γ and X_z and between X_x and X_y on the number of GaAs and AlAs layers, which can be understood by symmetry considerations derived from the perfect superlattices. The results form the basis for further exploration of the imperfection of the interface.

ACKNOWLEDGMENTS

One of us (L.J.S.) wishes to thank R. E. Nahory, M.-H. Meynadier, and M. Sturge for stimulating discussions. This work was supported by the National Science Foundation (NSF) under Grant No. DMR-88-15068.

[1]A. Ishibashi, Y. Mori, M. Itahashi, and N. Watanabe, J. Appl. Phys. **58**, 2691 (1985).

[2]D. J. Wolford, T. F. Keuch, J. A. Bradley, M. A. Gell, D. Ninno, and M. Jaros, J. Vac. Sci. Technol. B **4**, 1043 (1986); M. A. Gell, D. Ninno, M. Jaros, D. J. Wolford, T. F. Keuch, and J. A. Bradley, Phys. Rev. B **35**, 1196 (1987).

[3]E. Finkman, M. D. Sturge, and M. C. Tamargo, Appl. Phys. Lett. **49**, 1299 (1986); M. C. Tamargo, R. E. Nahory, M.-H. Meynadier, E. Finkman, M. D. Sturge, D. M. Hwang, and J. Ihm, J. Cryst. Growth **81**, 109 (1987); E. Finkman, M. D. Sturge, M.-H. Meynadier, R. E. Nahory, M. C. Tamargo, D. M. Hwang, and C. C. Chang, J. Lumin. **39**, 57 (1988); M. D. Sturge, E. Finkman, and M. C. Tamargo, J. Lumin. **40**, 425 (1988).

[4]G. Danan, B. Etienne, F. Mollot, R. Planel, A. M. Jean-Louis, F. Alexandre, B. Jusserand, G. Le Roux, J. Y. Marzin, H. Savary, and B. Sermage, Phys. Rev. B **35**, 6207 (1987).

[5]G. Danan, F. R. Ladan, F. Mollot, and R. Planal, J. Phys. (Paris) Colloq. **48**, C5-499 (1987).

[6]J. Nagle, M. Garriga, W. Stolz, T. Isu, and K. Ploog, J. Phys. (Paris) Colloq. **48**, C5-495 (1987); T. Isu, De-Sheng Jiang, and K. Ploog, Appl. Phys. A **43**, 75 (1987).

[7]F. Minami, K. Hirata, R. Era, T. Yao, and Y. Masumoto, Phys. Rev. B **36**, 2875 (1987).

[8]M.-H. Meynadier, R. E. Nahory, J. M. Workock, M. C. Tamargo, J. L. de Miguel, and M. D. Sturge, Phys. Rev. Lett. **60**, 1338 (1988).

[9]J. E. Golub, P. F. Liao, D. J. Eilenberger, J. P. Harbison, L. T. Florez, and Y. Prior, Appl. Phys. Lett. **53**, 2584 (1988).

[10]K. J. Moore, P. Dawson, and C. T. Foxon, Phys. Rev. B **38**, 3368 (1988); K. J. Moore, G. Duggan, P. Dawson, and C. T. Foxon, *ibid.* **38**, 5535 (1988).

[11]H. W. van Kesteren, E. C. Cosman, F. J. A. M. Greidanus, P. Dawson, K. J. Moore, and C. T. Foxon, Phys. Rev. Lett. **61**, 129 (1988).

[12]B. A. Wilson, C. E. Bonner, R. C. Spitzer, P. Dawson, K. J. Moore, and C. T. Foxon, J. Vac. Sci. Technol. B **6**, 1156 (1988).

[13]K. Imanishi, H. Fujimoto, T. Nakazawa, K. Taniguchi, C. Hamaguchi, and S. Sasa, in *Proceedings of the 19th International Conference on the Physics of Semiconductors,* edited by W. Zawadzki (Polish Academy of Sciences, Warsaw, 1988), p. 381.

[14]B. Gil, P. Lefebvre, H. Mathieu, F. Mollot, and R. Planel, in Ref. 13, p. 365.

[15]F. Minami, K. Todori, and K. Inoue, in Ref. 13, p. 411.

[16]J. N. Schulman and T. C. McGill, Phys. Rev. Lett. **39**, 1681 (1977); Phys. Rev. B **19**, 6341 (1979); J. Vac. Sci. Technol. **15**, 1456 (1978); Phys. Rev. B **23**, 4149 (1981).

[17]E. Caruthers and P. J. Lin-Chung, Phys. Rev. B **17**, 2705

(1978).
[18]G. C. Osbourn and D. L. Smith, Phys. Rev. B **19**, 2124 (1979).
[19]W. Andreoni and R. Car, Phys. Rev. B **21**, 3334 (1980).
[20]J. N. Schulman and Y.-C. Chang, Phys. Rev. B **24**, 4445 (1981); Phys. Rev. B **31**, 2059 (1985); **31**, 2069 (1985).
[21]J. Sanchez-Dehesa and C. Tejedor, Phys. Rev. B **26**, 5824 (1982).
[22]T. Nakayama and H. Kamimura, J. Phys. Soc. Jpn. **54**, 4726 (1985).
[23]H. Kamimura and T. Nakayama, in *Proceedings of the 18th International Conference on the Physics of Semiconductors,* edited by O. Engström (World Scientific, Singapore, 1987), p. 643.
[24]N. E. Christensen, E. Molinari, and G. B. Bachelet, Solid State Commun. **56**, 125 (1985).
[25]M. A. Gell, D. Ninno, M. Jaros, and D. C. Herbert, Phys. Rev. B **34**, 2416 (1986); M. A. Gell and D. C. Herbert, *ibid.* **35**, 9591 (1987).
[26]H. Rücker, M. Hanke, F. Bechstedt, and R. Enderlein, Superlatt. Microstruct. **2**, 477 (1986).
[27]J. Ihm, Appl. Phys. Lett. **50**, 1068 (1987).
[28]L. Brey and C. Tejedor, Phys. Rev. B **35**, 9112 (1987).
[29]D. Z.-Y. Ting and Y.-C. Chang, Phys. Rev. B **36**, 4359 (1987).
[30]I. P. Batra, S. Ciraci, and J. S. Nelson, J. Vac. Sci. Technol. B **5**, 1300 (1987).
[31]D. M. Bylander and L. Kleinman, Phys. Rev. B **36**, 3229 (1987).
[32]S.-H. Wei and A. Zunger, J. Appl. Phys. **63**, 5795 (1988).
[33]Y. Hatsugai and T. Fujiwara, Phys. Rev. B **37**, 1280 (1988).
[34]S. Massidda, B. I. Min, and A. J. Freeman, Phys. Rev. B **38**, 1970 (1988).
[35]Jian-Bai Xia, Phys. Rev. B **38**, 8358 (1988).
[36]B. A. Wilson, IEEE Quantum Electron. **QE-24**, 1763 (1988).
[37]R. W. Godby, M. Schlüter, and L. J. Sham, Phys. Rev. B **37**, 10 159 (1988).
[38]G. F. Koster, in *Solid State Physics,* edited by H. Ehrenreich, F. Seitz, and D. Turnbull (Academic, New York, 1957), Vol. 5, p. 174.
[39]J. Zak, A. Casher, M. Glück, and Y. Gur, *The Irreducible Representations of Space Groups* (Benjamin, New York, 1969).
[40]J. C. Slater and G. F. Koster, Phys. Rev. **94**, 1498 (1954).
[41]P.-O. Löwdin, J. Chem. Phys. **18**, 365 (1950).
[42]P. Vogl, H. Hjalmarson, and J. D. Dow, J. Phys. Chem. Solids **44**, 365 (1983).
[43]*Landolt-Börnstein: Numerical Data and Functional Relationships in Science and Technology* (New Series), edited by O. Madelung (Springer-Verlag, Berlin, 1987), Vol. III/22a, pp. 63 and 82.
[44]A. A. Kopylov, Solid State Commun. **56**, 1 (1985).
[45]R. C. Miller, D. A. Kleinman, and A. C. Gossard, Phys. Rev. B **29**, 7085 (1984).
[46]G. A. Sai-Halasz, L. Esaki, and W. A. Harrison, Phys. Rev. B **18**, 2812 (1978).
[47]S. R. White, G. E. Marques, and L. J. Sham, J. Vac. Sci. Technol. **21**, 544 (1982).
[48]See, for example, I. Umebu, S. Komiya, T. Nakamura, S. I. Mutoh, and A. Iida, J. Phys. (Paris) Colloq. **48**, C5-41 (1987).